Research Article

Environmental Chemistry and Safety
DOI: 10.26599/ECS.2025.9600026
2025, 1, 9600026

Predictive modeling of micropollutant removal in fixed-bed adsorbers

Maria N. Zarcheva[1] and Khim Hoong Chu[2*]

[1]Sofia University, Faculty of Mathematics and Informatics, 1164 Sofia, Bulgaria

[2]Institute of Energy Infrastructure, Universiti Tenaga Nasional (UNITEN), Kajang 43000, Selangor, Malaysia

Abstract: Fixed-bed adsorption is a promising technology for removing micropollutants from water, and its performance can be predicted using mechanistic models. Predictive modeling, however, is often hindered by the need for extensive parameter estimation. This study adopted a methodology that minimized experimental input and avoided calibration against breakthrough data. Three constant pattern models were evaluated: (1) an irreversible isotherm with film and intraparticle diffusion, (2) an irreversible isotherm with intraparticle diffusion only, and (3) a Langmuir isotherm with intraparticle diffusion only. Equilibrium parameters were obtained from batch adsorption experiments, and transport parameters were estimated from literature correlations. The models were tested against two published breakthrough datasets: ciprofloxacin on a polymeric resin and phenol on activated carbon. For the ciprofloxacin-resin system, only the model including both film and intraparticle diffusion resistances yielded quantitative agreement with the data. For the phenol-carbon system, none of the models reproduced the breakthrough curve, indicating underestimation of the intraparticle diffusion coefficient by the correlation. Agreement was recovered when a higher diffusion coefficient was assumed. These results demonstrate the limitations of current correlations and highlight the need for improved predictive tools for intraparticle diffusion in adsorption systems.

Key words: Constant pattern; Linear driving force; Cooper model; Hall model; Yoshida model

Citation: Zarcheva M N., Chu K H. Predictive modeling of micropollutant removal in fixed-bed adsorbers. *Environmental Chemistry and Safety*, 2025, 1, 9600026. https://doi.org/10.26599/ECS.2025.9600026

1. Introduction

Municipal wastewater treatment plants are not designed to fully eliminate trace organic contaminants. As a result, a wide spectrum of micropollutants, including pharmaceuticals, personal care products, and industrial chemicals, frequently persist through conventional treatment processes. These compounds, often detected in treated effluents at concentrations from ng L^{-1} to μg L^{-1}, are discharged into receiving waters, where they may disrupt aquatic ecosystems and pose risks to human health through long-term exposure [1]. Their persistence highlights the urgent need for effective post-treatment technologies.

Adsorption has emerged as one of the most promising strategies for this purpose. Granular activated carbon (GAC), in particular, has long been the adsorbent of choice in the water industry. Pilot-scale demonstrations have shown that fixed-bed GAC adsorbers can reliably remove a broad range of micropollutants [2, 3]. Compared with advanced oxidation processes and membrane filtration, adsorption offers a simpler and less energy-intensive option. Nevertheless, adsorption has also been integrated with these more complex processes in hybrid systems, yielding enhanced overall treatment performance [4, 5]. Beyond its established role in practice, research continues to explore advanced adsorbents engineered to surpass GAC in terms of adsorption capacity, selectivity, or regeneration potential. Such materials are typically evaluated in fixed-bed configurations, with breakthrough experiments serving as the key benchmark for performance assessment.

Mechanistic fixed-bed models play a central role in interpreting breakthrough experiments and in guiding process design and scale-up. As outlined in Ruthven's monograph [6], a physically realistic model must represent the fundamental processes that govern breakthrough curve behavior: adsorption thermodynamics, axial dispersion, external film mass transfer, and intraparticle diffusion. The latter may proceed via pore diffusion or surface (solid) diffusion, and in cases of physical adsorption, surface binding kinetics are usually assumed to be fast relative to these transport processes. By accounting for these mechanisms, such models provide a quantitative link between laboratory-scale measurements and practical system performance.

In contrast, conventional process design and scale-up methods rely heavily on empirical correlations that conflate equilibrium and kinetic effects into parameters fitted from pilot-scale breakthrough data. These correlations are inherently system-specific, offering minimal predictive value beyond the conditions under which they were derived. Although they can reproduce pilot data, they are experimentally costly, provide limited mechanistic insight, and ultimately impede reliable scale-up.

For predictive modeling, it is critical that model parame-

Correspondence to: Chu K H, khimchu@gmail.com
Received: July 4, 2025; Revised: October 23, 2025; Accepted: November 4, 2025

ters be determined independently, rather than by direct fitting to breakthrough data [7–10]. In standard practice, correlations are used to estimate axial dispersion and external mass transfer coefficients, while intraparticle diffusion coefficients are obtained from independent uptake studies in batch systems, shallow beds, or micro-columns. Adsorption isotherms are usually derived from equilibrium batch tests. While this multistep workflow supports reliable predictions, it demands substantial experimental effort and can limit the pace of adsorbent development.

The objective of this study is to assess the feasibility of a streamlined predictive modeling approach. Specifically, we consider a scenario in which only equilibrium isotherms are obtained experimentally, while all transport-related parameters —including intraparticle diffusion coefficients —are estimated using engineering correlations. This "quick-and-dirty" methodology is evaluated using three mechanistic models against published breakthrough data for ciprofloxacin adsorption on a polymeric ion-exchange resin and phenol adsorption on activated carbon. Both compounds are widely recognized micropollutants of global concern [1], making them suitable test cases for assessing the capabilities and limitations of this simplified modeling framework.

2. Mechanistic Fixed-Bed Models

Mechanistic fixed-bed models that account for nonlinear adsorption, convection, axial dispersion, external mass transfer, and intraparticle diffusion generally require numerical solution methods. Under certain simplifying assumptions, however, analytical solutions can be derived. Such solutions are particularly useful because they (1) provide direct insight into how process variables, such as flow rate, bed depth, and particle size, influence breakthrough behavior, (2) enable rapid sensitivity analyses, and (3) serve as benchmarks for validating numerical simulations under idealized conditions.

A widely used simplification in analytical modeling is the assumption of an irreversible (rectangular) equilibrium isotherm, which approximates highly favorable adsorption systems [6, 11]. Another is the constant pattern assumption, which states that the solute concentration profile retains its shape while propagating through the bed at a constant velocity [6, 12]. This assumption, often valid for favorable isotherms, greatly reduces the mathematical complexity of breakthrough curve analysis. The distance required for a system to reach constant pattern behavior depends on the degree of isotherm nonlinearity as well as the influence of axial dispersion and mass transfer resistances; in strongly favorable systems, this distance is typically short.

In this study, we employ three analytical models: two with an irreversible isotherm and one with a Langmuir isotherm, all developed under the constant pattern framework. These models are used to assess the feasibility of predictive modeling with minimal experimental input, as outlined in the following sections.

2.1. Model of Yoshida et al.

Yoshida et al. [13] provided a summary of analytical solutions for breakthrough curves in systems governed by irreversible equilibrium isotherms. They presented both a general solution and a constant pattern solution for a model that incorporates external film mass transfer and intraparticle diffusion, with the latter represented using a linear driving force (LDF) approximation. In this section, we summarize their fixed-bed model and highlight the corresponding constant pattern solution.

We consider micropollutant adsorption in a column of length L packed with spherical adsorbent particles of radius r_p. Neglecting axial dispersion, the governing mass balances for the fluid phase (interstitial volume) and the solid phase (adsorbent particles) are expressed in Eqs. (1) and (2). Here, c and c^* denote the solute concentrations in the bulk fluid and at the particle surface, respectively; $\bar{q}$ and q^* are the average and surface concentrations in the adsorbed phase; ε is the bed void fraction; v is the interstitial velocity; ρ_p is the particle density; k_f is the external film mass transfer coefficient; k_p is the LDF rate coefficient for solid diffusion; t is time; and z is the axial coordinate.

$$v\frac{\partial c}{\partial z} + \frac{\partial c}{\partial t} + \rho_p\left(\frac{1-\varepsilon}{\varepsilon}\right)\frac{\partial \bar{q}}{\partial t} = 0 \tag{1}$$

$$\frac{\partial \bar{q}}{\partial t} = \frac{3k_f}{r_p\rho_p}\left(c - c^*\right) = k_p\left(q^* - \bar{q}\right) \tag{2}$$

Adsorption equilibrium is assumed to follow an irreversible step-function isotherm [Eq. (3)], relating the adsorbed-phase concentration to the inlet fluid concentration c_0. Here, q_0 denotes the maximum adsorbed concentration corresponding to c_0. The associated initial and boundary conditions are given in Eq. (4).

$$c = 0,\ q^* = 0;\ c > 0,\ q^* = q_0 \tag{3}$$

$$\begin{aligned} t &= 0,\ c = \bar{q} = 0 \\ z &= 0,\ c = c_0 \end{aligned} \tag{4}$$

Under constant pattern conditions, the fixed-bed model admits the analytical solution given by Eq. (5) for $\delta \geqslant 1$ and Eq. (6) for $\delta \leqslant 1$ [13]. The dimensionless parameters δ, τ, and ξ are defined in Eqs. (7)–(9). In Eq. (7), the LDF rate coefficient k_p is replaced by $15D_s/r_p^2$, with D_s representing the solid diffusion coefficient.

$$\frac{c}{c_0} = \frac{1}{\delta}\exp\left(\tau - \xi + \delta - 1 - \frac{1}{\delta}\right) \tag{5a}$$

$$\text{for } \tau - \xi \leqslant -\delta + 1 + \frac{1}{\delta} - \ln\left(\frac{1+\delta}{\delta}\right)$$

$$\frac{c}{c_0} = 1 - \frac{\delta}{1+\delta}\exp\left\{\frac{1}{\delta}\left[-\tau + \xi - \delta + 1 + \frac{1}{\delta} - \ln\left(\frac{1+\delta}{\delta}\right)\right]\right\} \tag{5b}$$

$$\text{for } \tau - \xi \geqslant -\delta + 1 + \frac{1}{\delta} - \ln\left(\frac{1+\delta}{\delta}\right)$$

$$\frac{c}{c_0} = \exp\left(\tau - \xi - 1\right) \tag{6a}$$

for $\tau - \xi \leqslant 1 - \ln(1+\delta)$

$$\frac{c}{c_0} = 1 - \frac{\delta}{1+\delta}\exp\left\{\frac{1}{\delta}\left[-\tau + \xi + 1 - \ln(1+\delta)\right]\right\} \quad (6b)$$

for $\tau - \xi \geqslant 1 - \ln(1+\delta)$

$$\delta = \frac{1}{5}\frac{k_f r_p}{D_s}\frac{c_0}{\rho_p q_0} \quad (7)$$

$$\tau = \frac{3k_f}{r_p}\frac{c_0}{\rho_p q_0}\left(t - \frac{L}{v}\right) \quad (8)$$

$$\xi = \frac{3k_f}{r_p}\frac{L}{v}\left(\frac{1-\varepsilon}{\varepsilon}\right) \quad (9)$$

2.2. Model of Cooper

The second model, proposed by Cooper [14], also assumes irreversible adsorption under constant pattern conditions. In this case, only intraparticle solid diffusion is considered rate-limiting, again represented by the LDF approximation. Accordingly, Eq. (2) is replaced by Eq. (10), where $k_p = 15D_s/{r_p}^2$. The governing equations are represented by Eqs. (1), (3), (4), and (10), with the analytical solution given in Eq. (11). The associated dimensionless parameters ξ_p and τ_p are defined in Eqs. (12) and (13). This formulation is reported in Ruthven's monograph [6].

$$\frac{\partial \bar{q}}{\partial t} = k_p\left(q^* - \bar{q}\right) \quad (10)$$

$$\frac{c}{c_0} = 1 - \xi_p \exp\left(-\tau_p\right) \quad (11a)$$

for $\xi_p \leqslant 1$

$$\frac{c}{c_0} = 1 - \exp\left(\xi_p - \tau_p - 1\right) \quad (11b)$$

for $1 \leqslant \xi_p \leqslant 1 + \tau_p$

$$\tau_p = \frac{15D_s}{{r_p}^2}\left(t - \frac{L}{v}\right) \quad (12)$$

$$\xi_p = \frac{15D_s}{{r_p}^2}\frac{\rho_p q_0}{c_0}\frac{L}{v}\left(\frac{1-\varepsilon}{\varepsilon}\right) \quad (13)$$

2.3. Model of Hall et al.

The third model, originally formulated by Glueckauf and Coates [15] and generalized by Hall et al. [16], also assumes intraparticle diffusion as the rate-limiting step under constant pattern conditions, with solid diffusion described by the LDF approximation. Unlike the Yoshida and Cooper models, however, equilibrium is represented by a Langmuir isotherm rather than an irreversible step function. Specifically, Eq. (3) is replaced by Eq. (14), where q_m is the maximum adsorption capacity and b is the Langmuir equilibrium constant. The governing equations are Eqs. (1), (4), (10), and (14). The analytical solution, referred to as the Hall model, is given in Eq. (15), with the dimensionless parameters T, N, and r defined in Eqs. (16)–(18), and the isotherm correction factor ψ defined in Eq. (19) [16]. The formulation used here follows the version presented by LeVan et al. [12].

$$q^* = \frac{q_m b c}{1 + bc} \quad (14)$$

$$N(T-1) = \frac{1}{1-r}\ln\left[\frac{(c/c_0)^r}{1 - c/c_0}\right] - 1 \quad (15)$$

$$T = \frac{c_0}{\rho_p q_0}\left(\frac{vt}{L} - 1\right)\left(\frac{\varepsilon}{1-\varepsilon}\right) \quad (16)$$

$$N = \frac{15\psi D_s}{r_p^2}\frac{\rho_p q_0}{c_0}\frac{L}{v}\left(\frac{1-\varepsilon}{\varepsilon}\right) \quad (17)$$

$$r = \frac{1}{1 + bc_0} \quad (18)$$

$$\psi = \frac{1}{r^{1.06} + 1.125(1-r)^{1.06}} \quad (19)$$

2.4. Model evaluation and fitting

All model predictions were generated in Microsoft Excel. For cases requiring isotherm parameter estimation from experimental data, nonlinear regression was performed using GraphPad Prism.

3. Results and Discussion

The predictive capabilities of the Yoshida, Cooper, and Hall models were examined using published datasets on micropollutant adsorption in fixed-bed systems. As the Yoshida and Cooper models assume irreversible equilibrium behavior, a fundamental criterion for dataset selection was the presence of highly favorable adsorption isotherms, approaching the rectangular limit. Following an extensive literature review, two representative case studies were identified: (1) ciprofloxacin breakthrough on an ion-exchange resin [17], and (2) phenol removal in a fixed-bed column packed with GAC [18]. Both compounds have been classified as globally significant micropollutants in a comprehensive risk assessment [1].

It should be noted that the influent concentrations reported in the selected studies were in the mg L^{-1} range, reflecting adsorption as a primary treatment strategy rather than as a polishing or post-treatment measure. However, environmentally relevant micropollutant concentrations are typically in the ng L^{-1}–μg L^{-1} range, where adsorption isotherms can be approximated as linear. Under such conditions, the models evaluated here are not directly applicable. Nevertheless, suitable alternatives exist, since fixed-bed adsorption models admit analytical solutions in the linear isotherm limit, irrespective of kinetic complexity [6].

3.1. Prediction of ciprofloxacin breakthrough

In the first case study, ciprofloxacin removal in a fixed-bed column packed with the cation-exchange resin Supergel SGC650H (Purolite) was analyzed using experimental data from Sausen et al. [17]. Ciprofloxacin, a widely used fluoroquinolone antibiotic, is excreted largely unmetabolized and is poorly removed by conventional wastewater treatment, leading to its frequent detection in natural and drinking water sources. As a micropollutant, it remains biologically active at trace levels and contributes to the spread of antibiotic resistance.

Fig. 1 shows the experimental isotherm for the ciprofloxacin-resin system, obtained from batch experiments at 30°C and an initial pH of 5. In these experiments, ciprofloxacin hydrochloride solutions were contacted with resin particles in agitated flasks for 48 hours. Fig. 1 shows that the Langmuir model effectively describes the near-rectangular isotherm, capturing both the steep initial rise and the plateau (R^2 = 0.908, q_m = 515.3 mg g^{-1}, b = 1951 cm^3 mg^{-1}). Fixed-bed experiments were subsequently performed at 30°C using a jacketed glass column (30 cm height, 1 cm diameter). A ciprofloxacin solution (0.1 mg cm^{-3}, pH 5) was fed through the column under varying flow rates and packed-bed lengths. The selected breakthrough curve was obtained from a 7.6 cm packed column operated at 5 cm^3 min^{-1}, corresponding to an interstitial velocity of 8.38 cm min^{-1} and an empty bed contact time (EBCT) of 1.2 min.

Fig. 2 presents the experimental breakthrough curve, displaying a characteristic sigmoidal profile, with c/c_0 approaching unity within the experimental timeframe. The fixed-bed experiment was terminated after ~4500 minutes (3 days). The Yoshida prediction in Fig. 2 was generated using the parameters in Table 1, with key experimental conditions taken from the original study [17]. From Eq. (18), the separation factor r is 0.005, calculated using b = 1951 cm^3 mg^{-1} and c_0 = 0.1 mg cm^{-3}. According to Yoshida et al. [13], when r < 0.05, the isotherm may be approximated as rectangular with negligible error. This confirms that the assumption of irreversible adsorption, a prerequisite for applying the Yoshida model, is valid for the selected fixed-bed experiment.

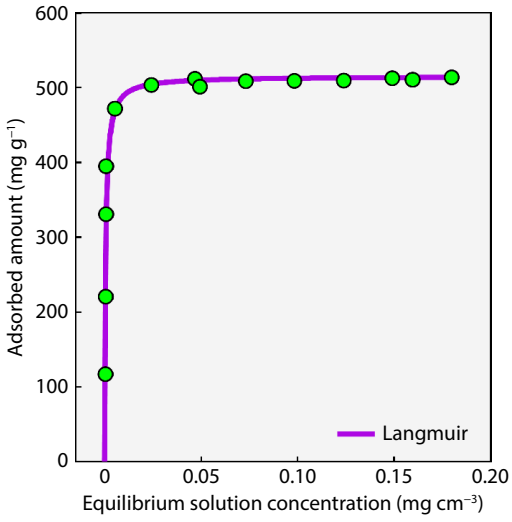

Fig. 1. Equilibrium adsorption of ciprofloxacin on ion-exchange resin Supergel SGC650H. Symbols: experimental data; solid line: Langmuir model. Data from Sausen et al. [17].

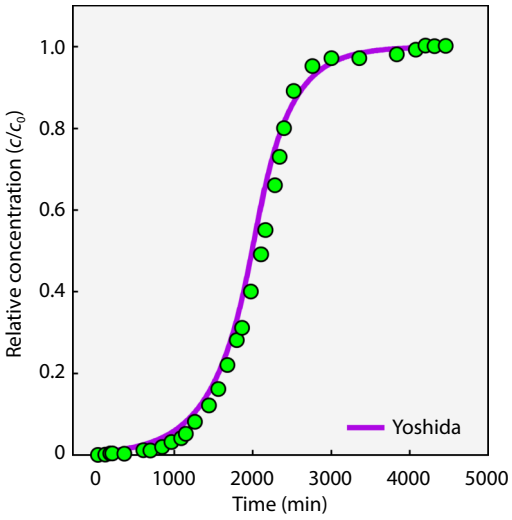

Fig. 2. Ciprofloxacin breakthrough on ion-exchange resin Supergel SGC650H (influent concentration: 0.1 mg cm^{-3}; flow rate: 5 cm^3 min^{-1}; packed-bed length: 7.6 cm). Symbols: experimental data; solid line: Yoshida model (parameters in Table 1). Data from Sausen et al. [17].

Table 1. Parameters for Yoshida, Cooper, and Hall predictions of ciprofloxacin breakthrough on ion-exchange resin Supergel SGC650H [17].

Parameter	Symbol	Value	Units
Packed-bed length	L	7.6	cm
Bed void fraction	ε	0.76	–
Interstitial velocity	v	8.38	cm min^{-1}
Particle radius	r_p	0.0327	cm
Particle density	ρ_p	1.26	g cm^{-3}
Feed concentration	c_0	0.1	mg cm^{-3}
Maximum uptake	q_0	512.7	mg g^{-1}
Solid diffusion coefficient	D_s	1.82×10^{-7}	cm^2 min^{-1}
Film mass transfer coefficient	k_f	0.151	cm min^{-1}

The equilibrium uptake (q_0) in Table 1 was estimated from the Langmuir isotherm [Eq. (14)] by substituting c with c_0 and applying the fitted parameters q_m and b. Under the assumption of irreversible adsorption, q_0 is typically taken as q_m. For the near-rectangular isotherm in Fig. 1, the Langmuir-based estimate of q_0 is nearly identical to q_m. The film mass transfer coefficient (k_f) and solid diffusion coefficient (D_s) could, in principle, be obtained from experimental data; however, in line with the objective of minimizing parameter fitting, they were estimated using literature correlations. The relevant expressions are summarized below.

Due to the scarcity of engineering correlations, D_s is generally determined from kinetic experiments. An empirical correlation specific to organic pollutants proposed by Worch [19] is presented in Eq. (20). This expression relates D_s to the molecular diffusivity (D_0) and other system-specific parameters. To obtain D_s in units of m^2 s^{-1}, the required inputs are D_0 (m^2 s^{-1}), r_p (m), c_0 (mg L^{-1}), and q_0 (mg g^{-1}). Worch [19] also proposed a separate correlation for D_0 [Eq. (21)], which requires the temperature T (K), dynamic viscosity η (Pa·s), and solute molecular weight M (g mol^{-1}). The D_s value calculated using Eqs. (20) and (21) is reported in Table 1. It is important to note that the specified units must be strictly adhered to in both equations.

$$D_s = 8.6 \times 10^{-5} r_p \sqrt{\frac{D_0 c_0}{q_0}} \quad (20)$$

$$D_0 = \frac{3.595 \times 10^{-14} T}{\eta M^{0.53}} \quad (21)$$

Unlike the case of D_s, for which few correlations exist, several correlations are available for estimating k_f in packed beds, though they often yield divergent results. In this study, four literature correlations were evaluated: Eq. (22) from Williamson et al. [20], Eq. (23) from Wilson and Geankoplis [21]; Eq. (24) from Ohashi et al. [22], and Eq. (25) from Chatzopoulos and Varma [23]. Each correlation expresses k_f in terms of the Sherwood (*Sh*), Reynolds (*Re*), and Schmidt (*Sc*) numbers, defined in Eqs. (26)–(28), which depend on D_0, particle diameter (d_p), superficial velocity (u), and kinematic viscosity (ν). Higher *Re* (or flow velocity) or *Sh* values correspond to thinner external films and enhanced mass transfer, leading to sharper breakthrough fronts. Conversely, lower values indicate greater film resistance and more gradual breakthrough curves. The Schmidt number characterizes the influence of fluid properties, particularly viscosity and solute diffusivity, on k_f.

$$Sh = 2.4\varepsilon^{0.66} Re^{0.34} Sc^{0.42} \quad (22)$$

$$Sh = \frac{1.09}{\varepsilon} Re^{1/3} Sc^{1/3} \quad (23)$$

$$Sh = 2 + 1.58 Re^{0.4} Sc^{1/3} \quad (24)$$

$$Sh = 2 + 3.44 Re^{0.471} Sc^{1/3} \quad (25)$$

$$Sh = \frac{k_f d_p}{D_0} \quad (26)$$

$$Re = \frac{u d_p}{\nu} \quad (27)$$

$$Sc = \frac{\nu}{D_0} \quad (28)$$

The k_f values estimated from the Williamson and Chatzopoulos–Varma correlations are 0.215 and 0.205 cm min^{-1}, respectively, approximately twice those from the Wilson–Geankoplis and Ohashi correlations (0.083 and 0.101 cm min^{-1}). Given this variability, it is common practice to adopt an average value when no single correlation can be clearly preferred [24, 25]. Accordingly, a mean k_f of 0.151 cm min^{-1} was used in this study, as reported in Table 1.

The values of k_f and D_s, along with the other parameters listed in Table 1, were used in the Yoshida model to generate the prediction shown in Fig. 2. The model reproduces the experimental breakthrough curve with good accuracy, despite relying solely on independently determined parameters. Notably, only q_0 was derived from batch experiments, while k_f and D_s were estimated from literature correlations, underscoring the potential of this predictive approach to avoid labor-intensive kinetic measurements and parameter estimation.

For this system, because δ from Eq. (7) is 0.84 (< 1), the Yoshida prediction in Fig. 2 was calculated using Eq. (6) rather than Eq. (5). As discussed by Yoshida et al. [13], δ reflects the relative significance of film mass transfer versus intraparticle diffusion. Only when $\delta > 10$ can film resistance be considered negligible. Here, δ = 0.84 indicates that external film resistance should not be neglected, a contribution most evident in the early portion of the breakthrough curve.

The sensitivity of the Yoshida model to k_f was evaluated by comparing predictions using the lowest and highest correlation values —0.083 cm min^{-1} (Wilson–Geankoplis) and 0.215 cm min^{-1} (Williamson) —with all other parameters in Table 1 held constant. As shown in Fig. 3, the model is strongly dependent on k_f, with the lower value predicting higher effluent concentrations during early breakthrough and the higher value yielding a closer match to the experimental curve.

These results highlight the critical influence of external mass transfer during the early stages of breakthrough, where

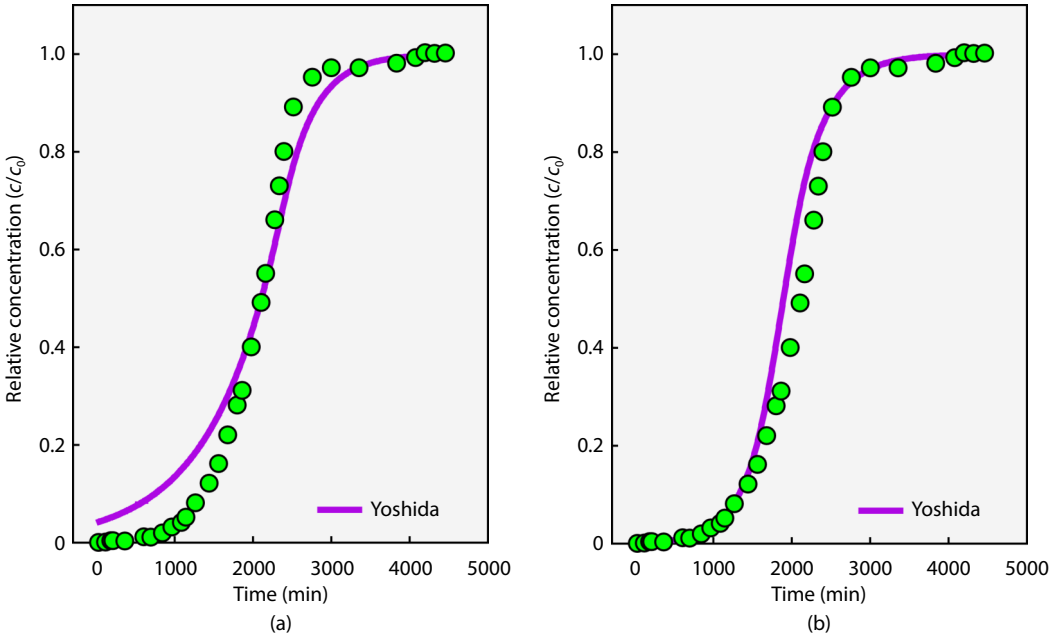

Fig. 3. Effect of k_f on Yoshida predictions for ciprofloxacin breakthrough on ion-exchange resin Supergel SGC650H. (a) k_f = 0.083 cm min^{-1}. (b) k_f = 0.215 cm min^{-1}. Data from Sausen et al. [17].

breakthrough time, a key design and operational parameter, is determined. For the ciprofloxacin-resin system, the predictive reliability of the Yoshida model depends strongly on k_f estimated from empirical correlations. Given the large variability among correlations, adopting a mean value provides a practical, though only partial, means of reducing this uncertainty.

In addition to k_f, the D_s value estimated from the Worch correlation [Eq. (20)] is a critical determinant of the agreement observed in Fig. 2, demonstrating the validity of the solid diffusion assumption in the Yoshida model. This assumption is consistent with the nature of the adsorbent, Supergel SGC650H, identified as a low-porosity gel-type cation-exchange resin [17], for which intraparticle transport is known to be governed primarily by solid diffusion [26]. Thus, the Yoshida model, which represents intraparticle transport solely by D_s, both accounts for the close agreement between prediction and experiment and affirms the appropriateness of the solid diffusion assumption for polymeric resins of this type.

The good agreement observed in Fig. 2 indicates that the solution environment in the fixed-bed experiment was comparable to that of the batch setup used to determine the equilibrium isotherm. In practice, however, water chemistry can evolve during extended fixed-bed operation. For instance, pH drift is common when unbuffered feed solutions are used. Because ciprofloxacin is an ionizable compound, its adsorption equilibrium and kinetics are highly sensitive to pH; even small shifts can markedly affect both uptake and transport behavior. Under such conditions, applying the q_0 value obtained from batch measurements would not yield reliable predictions. In the present case, the close correspondence between model prediction and experimental data suggests that no major pH drift occurred, despite the three-day operation. More broadly, variations in pH, ionic strength, and ion composition can substantially affect both equilibrium and mass transfer, particularly for ion-exchange resins where electrostatic interactions dominate. This underscores an important but often overlooked limitation in adsorption research: fixed-bed experiments are rarely conducted under controlled pH conditions, even though water chemistry can critically determine adsorption performance and model validity.

Like the Yoshida model, the Cooper model [Eq. (11)] assumes constant pattern behavior and irreversible adsorption. Its distinction lies in attributing adsorption kinetics to intraparticle transport via solid diffusion while neglecting external mass transfer. As shown in Fig. 4a, the Cooper model prediction based on the parameters in Table 1 deviates substantially from the experimental breakthrough curve, particularly in the early breakthrough region. This discrepancy likely stems from the omission of external film resistance. In contrast, the Yoshida model accurately reproduces the experimental breakthrough trend because it accounts for both film mass transfer and intraparticle diffusion. Although the Cooper model prediction could be improved by optimizing D_s, such empirical adjustment is unnecessary. Explicitly accounting for the film mass transfer mechanism, as in the Yoshida model, is sufficient to reproduce the experimental profile.

Fig. 4b shows the Hall prediction from Eq. (15), based on the parameters in Table 1 and the Langmuir constant (b = 1951 cm^3 mg^{-1}) for calculating the separation factor r in Eq. (18). Similar to the Cooper model, the Hall model is incapable of providing an accurate representation of the breakthrough data. This outcome is expected, as the Hall model also neglects external mass transfer resistance. Indeed, Fig. 4c shows that the Hall and Cooper predictions are virtually indistinguishable. This similarity stems from the near-rectangular isotherm (Fig. 1): for the ciprofloxacin-resin system, the separation factor is close to zero (r = 0.005). In this limit, the Langmuir equilibrium assumption of the Hall model effectively becomes equivalent to the irreversible equilibrium assumption of the Cooper model. In fact, setting $r = 0$ reduces the Hall model [Eq. (15)] to the Cooper model [Eq. (11)], with $N = \xi_p$ and $NT = \tau_p$ (with $\psi = 1$).

3.2. Prediction of phenol breakthrough

In the second case study, phenol adsorption on the commercial activated carbon Filtrasorb 400 (Calgon Carbon) was evaluated using experimental data from Otero et al. [18]. Although phenol is a long-established industrial pollutant and often excluded from discussions of emerging micropollutants, its environmental significance remains considerable. The global risk assessment by Yang et al. [1] identified phenol as a priority organic micropollutant in aquatic environments due to its persistence, widespread occurrence, and ecological risk.

Fig. 5 displays the experimental isotherm for the phenol-carbon system, obtained from batch experiments at 20°C. In

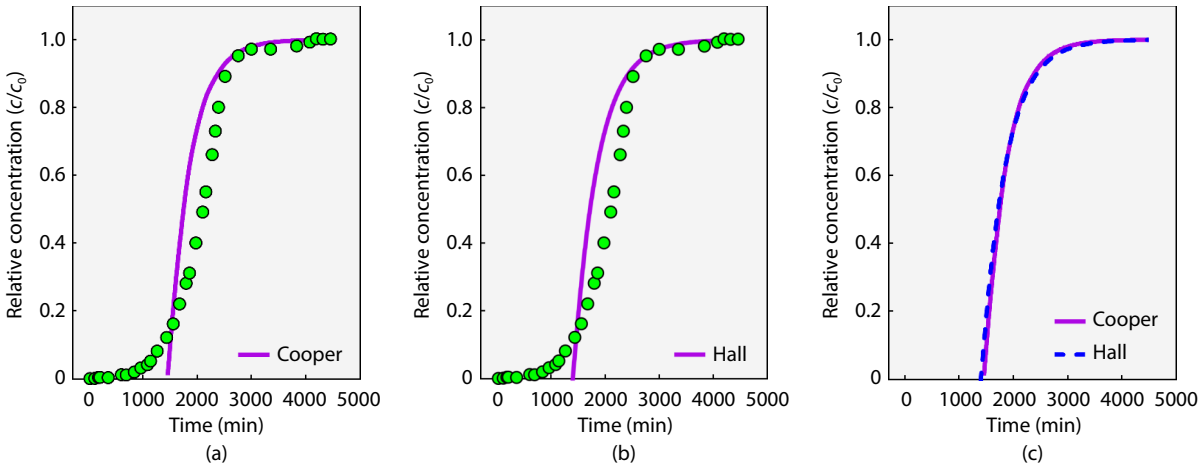

Fig. 4. Ciprofloxacin breakthrough on ion-exchange resin Supergel SGC650H. Symbols: experimental data; lines: model predictions (parameters in Table 1). (a) Cooper model. (b) Hall model. (c) Comparison of Cooper and Hall. Data from Sausen et al. [17].

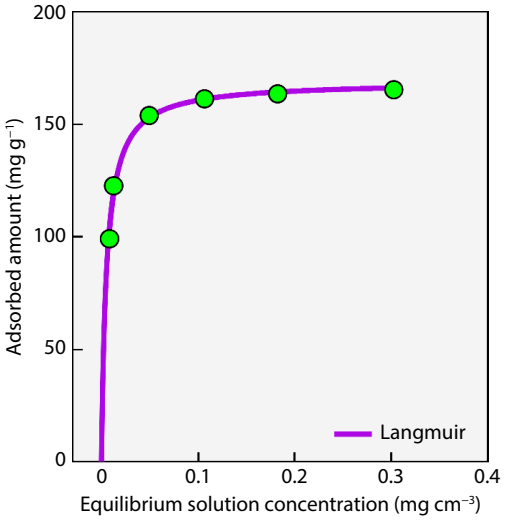

Fig. 5. Equilibrium adsorption of phenol on activated carbon Filtrasorb 400. Symbols: experimental data; solid line: Langmuir model. Data from Otero et al. [18].

these tests, samples of Filtrasorb 400 were equilibrated with phenol solutions under agitation for 48 hours. As shown in Fig. 5, the Langmuir model provides an excellent fit to the strongly favorable isotherm (R^2 = 0.992), yielding q_m = 169.1 mg g^{-1} and b = 193.4 cm^3 mg^{-1}. The chosen breakthrough curve was obtained from a column with an internal diameter of 1 cm and a packed-bed length of 10 cm. A phenol solution (0.1 mg cm^{-3}) was fed at 20°C and 10 cm^3 min^{-1}, corresponding to an EBCT of 0.8 min. For this feed concentration, the r value calculated from Eq. (18) is 0.05, which just meets the criterion (r < 0.05) for approximating the isotherm in Fig. 5 as rectangular.

Fig. 6a shows the experimental breakthrough profile, exhibiting only slight broadening. Also shown is the Yoshida prediction, obtained using the parameters listed in Table 2. The q_0 value in Table 2 was derived from the Langmuir isotherm based on the fitted q_m and b. The film mass transfer coefficient (k_f) was evaluated using four correlations [Eqs. (22)–(25)], with the estimated values spanning from 0.169 cm min^{-1} according to the Ohashi correlation to 0.358 cm min^{-1} based on the Chatzopoulos–Varma correlation. The k_f reported in Table 2 represents the average of these estimates. The solid diffusion coefficient (D_s) was calculated using the Worch correlation [Eq. (20)].

As shown in Fig. 6a, the Yoshida prediction diverges markedly from the sharp experimental profile. For this system, δ from Eq. (7) is 3.6 (> 1), Eq. (5) was therefore used to gener-

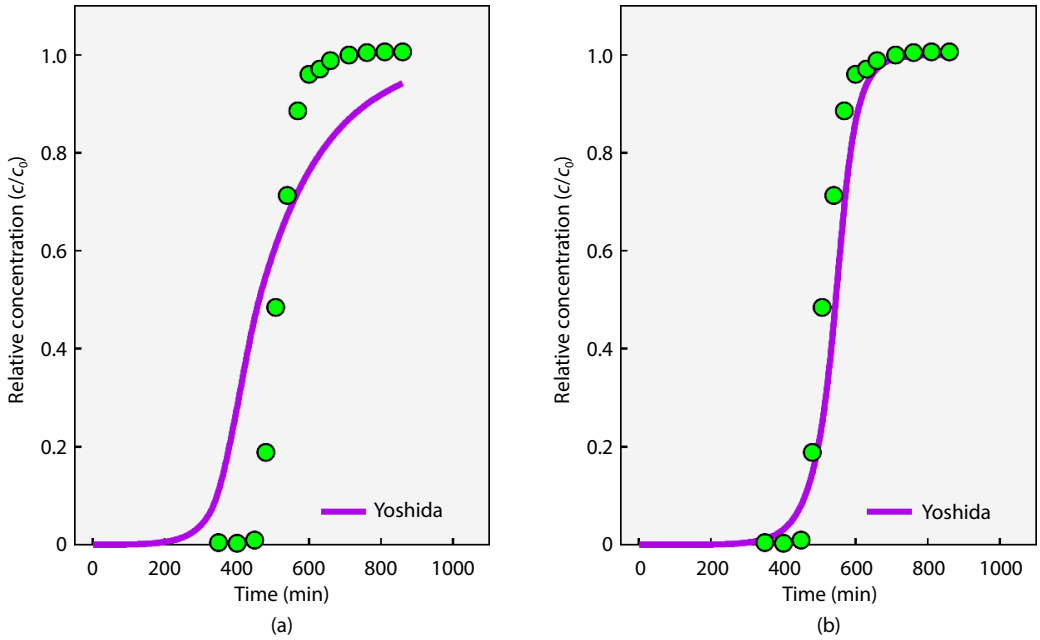

Fig. 6. Phenol breakthrough on activated carbon Filtrasorb 400 (influent concentration: 0.1 mg cm^{-3}; flow rate: 10 cm^3 min^{-1}; packed-bed length: 10 cm). Symbols: experimental data; solid lines: Yoshida model (parameters in Table 2). (a) Original parameters. (b) Same parameters as in (a), with D_s = 2.19 × 10^{-6} cm^2 min^{-1}. Data from Otero et al. [18].

Table 2. Parameters for Yoshida, Cooper, and Hall model predictions of phenol breakthrough on activated carbon Filtrasorb 400 [18].

Parameter	Symbol	Value	Units
Packed-bed length	L	10	cm
Bed void fraction	ε	0.4	–
Interstitial velocity	v	31.83	cm min^{-1}
Particle radius	r_p	0.035	cm
Particle density	ρ_p	0.7	g cm^{-3}
Feed concentration	c_0	0.1	mg cm^{-3}
Maximum uptake	q_0	160.8	mg g^{-1}
Solid diffusion coefficient	D_s	4.38 × 10^{-7}	cm^2 min^{-1}
Film mass transfer coefficient	k_f	0.253	cm min^{-1}

ate the model prediction. Because $\delta < 10$, the breakthrough behavior is expected to be governed by both external mass transfer and intraparticle diffusion. However, given the rapid increase in effluent concentration during the initial breakthrough, the effects of external mass transfer can be deemed negligible for this system.

The model's inability to reproduce the steep experimental profile suggests that the D_s value obtained from the Worch correlation is inaccurate. As shown in Fig. 6b, increasing D_s from 4.38×10^{-7} to 2.19×10^{-6} cm^2 min^{-1} (a fivefold increase) brings the prediction into closer agreement with the data. While the Worch correlation proved adequate in the first case study, the results in Fig. 6 highlight its limitations for the phenol-carbon system. Given the extensive literature on phenol adsorption onto Filtrasorb 400, the D_s value from the Worch correlation should be benchmarked against reported values to assess its reliability.

A particularly relevant study is that of Ocampo-Pérez et al. [27], who investigated phenol adsorption on Filtrasorb 400 in a batch system, focusing on the relative roles of pore and solid diffusion. They found that solid diffusion was the dominant intraparticle transport mechanism, while pore diffusion played a secondary role despite the porous structure of the adsorbent. Notably, they reported that D_s varied with phenol loading, ranging from 8.28×10^{-7} to 3.35×10^{-6} cm^2 min^{-1} (a fourfold difference). The D_s value from the Worch correlation (4.38×10^{-7} cm^2 min^{-1}) is about half the lower limit of the range reported by Ocampo-Pérez et al. [27]. In contrast, the adjusted value that yielded the close agreement in Fig. 6b (2.19×10^{-6} cm^2 min^{-1}) lies well within this range. This analysis indicates that the Worch correlation may not be universally reliable, as it can underestimate D_s for the phenol-carbon system.

Panels a and b of Fig. 7 indicate that the Cooper and Hall models do not adequately describe the breakthrough data, similar to the Yoshida model in Fig. 6a, as they do not capture the steep rise of the experimental profile. Fig. 7c compares the Cooper and Hall predictions, revealing some differences, most evident in the initial breakthrough region. These discrepan-

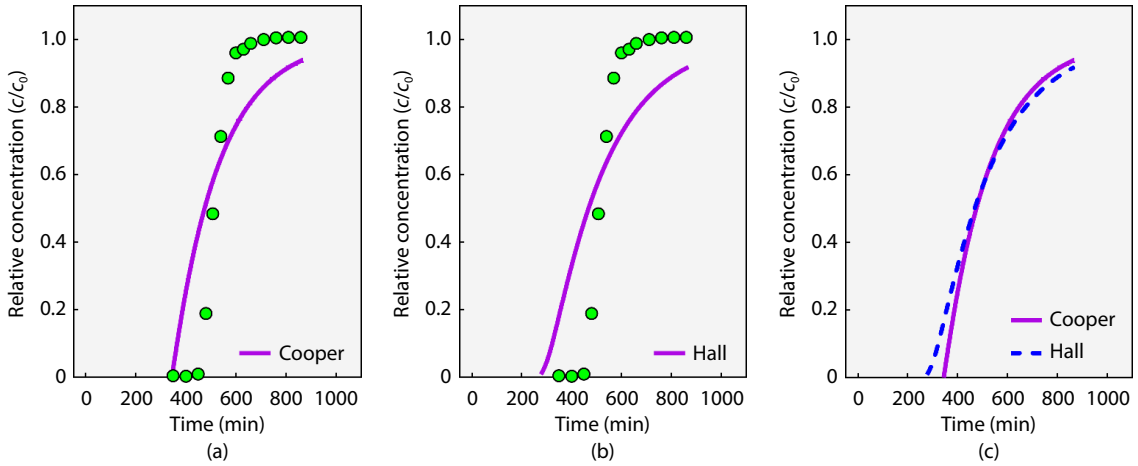

Fig. 7. Phenol breakthrough on activated carbon Filtrasorb 400. Symbols: experimental data; lines: model predictions (parameters in Table 2). (a) Cooper model. (b) Hall model. (c) Comparison of Cooper and Hall. Data from Otero et al. [18].

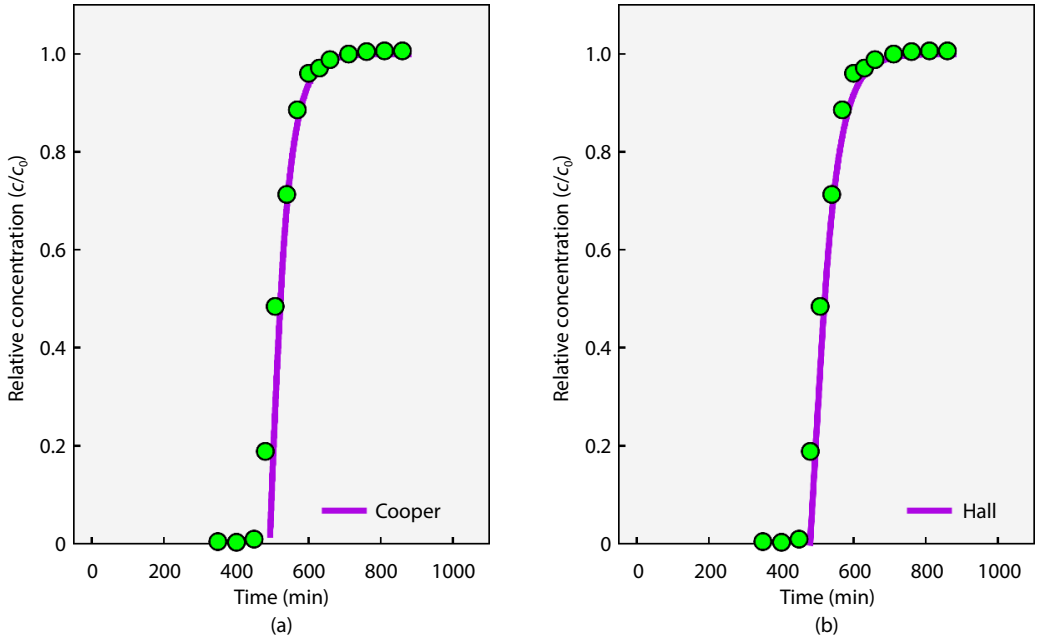

Fig. 8. Phenol breakthrough on activated carbon Filtrasorb 400. Symbols: experimental data; solid lines: model predictions (parameters in Table 2, with $D_s = 2.19 \times 10^{-6}$ cm^2 min^{-1}). (a) Cooper model. (b) Hall model. Data from Otero et al. [18].

cies likely arise from the departure of the experimental isotherm from the rectangular limit (Fig. 5). Under such conditions, the Langmuir equilibrium assumption underlying the Hall model is more appropriate than the irreversible assumption of the Cooper model.

Fig. 8 shows the Cooper and Hall predictions obtained using the same parameters as in Fig. 7, but with D_s replaced by the enhanced value of 2.19×10^{-6} cm^2 min^{-1}. These refined predictions align closely with the Yoshida result in Fig. 6b. Since the Cooper and Hall models neglect external mass transfer, their good agreement with the experimental data in Fig. 8 indicates that this mechanism is of secondary importance for this system.

4. Conclusions

This study investigated the predictive capabilities of the Yoshida, Cooper, and Hall models for fixed-bed adsorption of micropollutants under constant pattern conditions. The Yoshida model accounts for both external film and intraparticle diffusion, whereas the Cooper and Hall models consider only intraparticle diffusion. Equilibrium parameters were determined from batch experiments, while all mass transfer parameters, internal and external, were estimated from literature correlations, avoiding the need for kinetic experiments or parameter fitting.

Two case studies were examined: ciprofloxacin adsorption on a gel-type ion-exchange resin and phenol adsorption on activated carbon. For the ciprofloxacin-resin system, the Yoshida model reproduced the experimental breakthrough curve with good accuracy, while the Cooper and Hall models showed marked deviations due to their neglect of film mass transfer. For the phenol-carbon system, all three models underestimated the steepness of the breakthrough profile, primarily because the Worch correlation underestimated the solid diffusion coefficient (D_s). Satisfactory agreement was obtained only after increasing D_s to a value consistent with literature reports.

Overall, the results demonstrate both the utility and the limitations of correlation-based modeling. While such approaches can reduce experimental effort, their accuracy depends critically on the reliability of the underlying correlations, particularly for D_s. Future work should develop adsorbent-specific correlations for intraparticle diffusion and validate them through systematic breakthrough curve analysis.

CRediT authorship contribution statement

Maria N. Zarcheva: Formal analysis, Investigation, Writing – review & editing. **Khim Hoong Chu:** Conceptualization, Methodology, Writing – original draft, Writing – review & editing.

Declaration of competing interest

The authors declare no competing financial interest.

References

[1] Yang, Y.; Zhang, X.; Jiang, J.; Han, J.; Li, W.; Li, X.; Leung, K. M. Y.; Snyder, S. A.; Alvarez, P. J. J. Which micropollutants in water environments deserve more attention globally? *Environ. Sci. Technol.*, 2022, 56(1): 13–29.

[2] Benstoem, F.; Nahrstedt, A.; Boehler, M.; Knopp, G.; Montag, D.; Siegrist, H.; Pinnekamp, J. Performance of granular activated carbon to remove micropollutants from municipal wastewater—A meta-analysis of pilot- and large-scale studies. *Chemosphere*, 2017, 185: 105–118.

[3] Fundneider, T.; Acevedo Alonso, V.; Abbt-Braun, G.; Wick, A.; Albrecht, D.; Lackner, S. Empty bed contact time: The key for micropollutant removal in activated carbon filters. *Water Res.*, 2021, 191: 116765.

[4] Habagil, M.; Baresel, C.; Schleich, C.; Torisson, F.; Björksund-Tuominen, M.; Jönsson, K. Pilot trials with advanced water technologies to remove micropollutants from wastewater and assessment of the technologies for wastewater reuse in public blue-green solutions. *Water Pract. Technol.*, 2025, 20(5): 1306–1320.

[5] Núñez-Tafalla, P.; Salmerón, I.; Venditti, S.; Hansen, J. Exploring large pilot-scale applications of advanced oxidation and GAC filtration for removing micropollutants: Assessment of elimination efficiency and risk reduction. *Process Saf. Environ. Prot.*, 2025, 197: 106956.

[6] Ruthven, D. M. *Principles of Adsorption and Adsorption Processes*. New York: Wiley, 1984.

[7] Spahn, H.; Schlünder, E. U. The scale-up of activated carbon columns for water purification, based on results from batch tests—I. Theoretical and experimental determination of adsorption rates of single organic solutes in batch tests. *Chem. Eng. Sci.*, 1975, 30(5–6): 529–537.

[8] Brauch, V.; Schlünder, E. U. The scale-up of activated carbon columns for water purification, based on results from batch tests—II. Theoretical and experimental determination of breakthrough curves in activated carbon columns. *Chem. Eng. Sci.*, 1975, 30(5–6): 539–548.

[9] Crittenden, J. C.; Weber Jr, W. J. Predictive model for design of fixed-bed adsorbers: Parameter estimation and model development. *J. Environ. Eng. Div.*, 1978, 104(2): 185–197.

[10] Liu, K.-T.; Weber Jr, W. J. Characterization of mass transfer parameters for adsorber modeling and design. *J. Water Pollut. Control Fed.*, 1981, 53(10): 1541–1550. https://www.jstor.org/stable/25041535

[11] Chu, K. H. Fixed bed adsorption of water contaminants: A cautionary guide to simple analytical models and modeling misconceptions. *Sep. Purif. Rev.*, 2023, 52: 75–97.

[12] LeVan, M. D.; Carta, G.; Ritter, J. A.; Walton, K. S. Adsorption and ion exchange. In: *Perry's Chemical Engineers' Handbook*, 9th ed. Green, D. W., Southard, M. Z., Eds. New York: McGraw-Hill Education, 2019.

[13] Yoshida, H.; Kataoka, T.; Ruthven, D. M. Analytical solution of the breakthrough curve for rectangular isotherm systems. *Chem. Eng. Sci.*, 1984, 39(10): 1489–1497.

[14] Cooper, R. S. Slow particle diffusion in ion exchange columns. *Ind. Eng. Chem. Fund.*, 1965, 4(3): 308–313.

[15] Glueckauf, E.; Coates, J. I. Theory of chromatography. Part IV. The influence of incomplete equilibrium on the front boundary of chromatograms and on the effectiveness of separation. *J. Chem. Soc.*, 1947: 1315–1321.

[16] Hall, K. R.; Eagleton, L. C.; Acrivos, A.; Vermeulen, T. Pore- and solid-diffusion kinetics in fixed-bed adsorption under constant-pattern conditions. *Ind. Eng. Chem. Fund.*, 1966, 5(2): 212–223.

[17] Sausen, M. G.; Scheufele, F. B.; Alves, H. J.; Vieira, M. G. A.; da Silva, M. G. C.; Borba, F. H.; Borba, C. E. Efficiency maximization of fixed-bed adsorption by applying hybrid statistical-phenomenological modeling. *Sep. Purif. Technol.*, 2018, 207: 477–488.

[18] Otero, M.; Zabkova, M.; Rodrigues, A. E. Adsorptive purification of phenol wastewaters: Experimental basis and operation of a parametric pumping unit. *Chem. Eng. J.*, 2005, 110(1–3): 101–111.

[19] Worch, E. *Adsorption Technology in Water Treatment: Funda-*

mentals, Processes, and Modeling, 2nd ed. Berlin: Walter de Gruyter, 2021.

[20] Williamson, J. E.; Bazaire, K. E.; Geankoplis, C. J. Liquid-phase mass transfer at low Reynolds numbers. *Ind. Eng. Chem. Fund.*, 1963, 2(2): 126–129.

[21] Wilson, E. J.; Geankoplis, C. J. Liquid mass transfer at very low Reynolds numbers in packed beds. *Ind. Eng. Chem. Fund.*, 1966, 5(1): 9–14.

[22] Ohashi, H.; Sugawara, T.; Kikuchi, K.-I.; Konno, H. Correlation of liquid-side mass transfer coefficient for single particles and fixed beds. *J. Chem. Eng. Jpn.*, 1981, 14(6): 433–438.

[23] Chatzopoulos, D.; Varma, A. Aqueous-phase adsorption and desorption of toluene in activated carbon fixed beds: Experiments and model. *Chem. Eng. Sci.*, 1995, 50(1): 127–141.

[24] Ko, D. C. K.; Porter, J. F.; McKay, G. Film-pore diffusion model for the fixed-bed sorption of copper and cadmium ions onto bone char. *Water Res.*, 2001, 35(16): 3876–3886.

[25] Lv, L.; Zhang, Y.; Wang, K.; Ray, A. K.; Zhao, X. S. Modeling of the adsorption breakthrough behaviors of Pb^{2+} in a fixed bed of ETS-10 adsorbent. *J. Colloid Interface Sci.*, 2008, 325(1): 57–63.

[26] Li, P.; SenGupta, A. K. Intraparticle diffusion during selective sorption of trace contaminants: The effect of gel versus macroporous morphology. *Environ. Sci. Technol.*, 2000, 34(24): 5193–5200.

[27] Ocampo-Pérez, R.; Leyva-Ramos, R.; Sanchez-Polo, M.; Rivera-Utrilla, J. Role of pore volume and surface diffusion in the adsorption of aromatic compounds on activated carbon. *Adsorption*, 2013, 19(5): 945–957.